Defence Science Journal, Vol. 68, No. 3, May 2018, pp. 316-325, DOI : 10.14429/dsj.68.12354

Development of Adaptive Threshold and Data Smoothening Algorithm for GPR Imaging

Prabhat Sharma[*], Bambam Kumar[#], and Dharmendra Singh[#]

[*]*DRDO-Instrument Research and Development Establishment, Dehradun – 248 008, India*
[#]*Department of Electronics and Communication Engineering, Indian Institute of Technology, Roorkee - 247 667, India*
[*]*E-mail: prabhat@irde.drdo.in*

ABSTRACT

There are many approaches available to separate the background and foreground in image processing applications. Currently, researchers are focusing on wavelet De-noising, curvelet threshold, Edge Histogram Descriptor threshold, Otsu thresholding, recursive thresholding and adaptive progressive thresholding. In fixed and predictable background conditions, above techniques separate background and foreground efficiently. In a common scenario, background reference is blind due to soil surface moisture content and its non-linearity. There are many methodologies proposed from time to time by researchers to solve this blind reference background separation. But challenges still now remain, because there are two major problems in ground penetrating radar imaging such as targets like ground enhances the false alarm and non-metallic target detection, where the threshold decision is a critical task. In this paper, a novel real time blind adaptive threshold algorithm is proposed for ground penetrating radar image processing. The blind threshold was decided to use normal random variable variance and image data variance. Further, the image was smoothened by random variance ratio to image data variance. Experimental results showed satisfactory results for the background separation and smoothening the targeted image data with the proposed algorithm.

Keywords: GPR; Normal random variable; Variance; Adaptive threshold; Smoothenting

1. INTRODUCTION

The main difficulties associated with thresholding such as in GPR imaging applications occur when the associated noise process is non-stationary, correlated and non-Gaussian. Other factors such as scattering, variance of gray levels within the object and the background, inadequate contrast, object shape and size non-commensurate with the scene are complicating thresholding operation. Various researchers[1-6] have proposed denoising algorithms to overcome/minimie these challenges by using wavelet, which is generally derived from the generalised Gaussian distribution. In these papers, Wiener filter based de-noising[1] has been compared with adaptive wavelet based de-noising[2-6] using peak signal to noise ratio (PSNR). In high level noisy environment, wavelet based de-noising PSNR is higher than Wiener filter based de-noising. But tackling noise in wavelet based de-noising limits the performance. Another approach of adaptive thresholding is integrated neighbourhood search[7], where image is segmented in the background and object region in a complex background environment. This thresholding approach is computationally faster and accurate, but the image resolution is poor. Two dimensional least mean squares (2D LMS) algorithm[8] is also another approach to extract the target feature adaptively from the wideband ground penetrating radar system. The limitation of this algorithm is that it is not capable to discriminate the target/ natural clutter or target/anthropic clutter. Adaptive Thresholding Technique for Document Image Analysis[9] uses the global and local statistics by selecting the appropriate window for contrast stretching. This method is robust for document images, but selection of window for thresholding is the main limitation of this method. When the background is uneven in image then the variational method of adaptive thresholding[10-11] is suitable for finding the boundaries of the object by setting the only one parameter for variable threshold. This algorithm can remove the noise influence in the image, but high iteration time for convergence and noise level limit the performance of variational method. Block-median pyramidal transform[12] is a nonlinear multiscale pyramidal transform based on non-overlapping blocks decompositions using the median operation and a polynomial approximation for image de-noising. But this image de-noising method is applicable only when noise is independent and identically distributed (i.i.d) in nature. Zhang[14], *et al.* characterised the GPR data in three regions: singular, stationary region, which is the background and the transition region i.e. in-between. These characterisations have been done by adaptive 2-D entropy thresholding and OTSU method. But data homogeneity and stationary background are limiting factors of this method because data homogeneity and background conditions depend on soil and target characteristics (i.e. Terrain behaviour and target behaviour). Wu[15], *et al.* analysed the GPR

Received : 21 November 2017, Revised : 18 January 2018
Accepted : 12 February 2018, Online published : 16 April 2018

data using non-sampled contourlet transform and developed an adaptive threshold algorithm based on energy coefficient of GPR data for multiscale. This algorithm is a modification of wavelet thresholding and is performance limited by the strong noise environment. Nabelek[16], *et al.* used non-negative matrix factorisation (NMF) in GPR to improve the detection of deeply buried non-metal objects. In this approach, the GPR signal return is interpreted as the sum of two independent components from two different sources, the background and the object with a detection confidence. This approach, however, is not adaptive and it is an extension of principal component analysis. Abeynayake[17], *et al.* made up multiple background models for a variety of soil moisture levels to separate out the target response and background response from GPR response. If the test site is different from the predefined background models, then false alarm will increase. Zhang[18], *et al.* used the curvelet transform threshold with Bayes shrink to remove the environmental noise, systematic noise, other radio frequency interference signals and strong clutters in GPR. This approach is limited by the standard deviation of ground surface in GPR measurement. Kalika[19] used the mean and standard deviation normalisation, under the assumption that data with explosive threats have different statistical characteristics than the background/clutter; after normalisation, explosive threat data will have larger absolute normalised scores than the background/clutter. There is no adaptiveness, however, in this approach. Kenneth[20], *et al.* used Bayesian statistics and student distribution to select the threshold to separate background and foreground from the GPR data. This Bayesian approach gives superior performance for all fixed guard-band sizes. Hichem[21], *et al.* used an adaptive Edge Histogram Descriptor (EHD) to identify non-edge locations in the EHD feature extraction with the different edge types (vertical, horizontal, diagonal, and anti-diagonal), which have different dynamic ranges. This descriptor is capable of removing the soil specific edge background noise, which limit the performance of adaptive EHD.

So far, reported methods do not have sufficient capability to decide the threshold either to metallic target or for non-metallic target in GPR images, because each tested area has a blind threshold value. Under testing area, the nature of the ground changes the variance at each observation point and the buried object characteristics also change the variance of observing area. Till now variance approach has not been undertaken carefully. Due to the complex nature of the ground, it is very difficult to enhance the detection accuracy and reduce the false detection. Therefore, in this paper, an adaptive thresholding algorithm is proposed to separate the background and foreground for GPR image processing applications.

2. EXPERIMENTAL SETUP AND DATA COLLECTION

A GPR setup has been developed for detecting metallic and non-metallic targets as shown in Fig. 1. Overall experiment detail and developed SFCW GPR specifications show in Table 1. These specifications are shown for air as a medium. In present case soil moisture variation is from 5 per cent to 15 per cent for which dielectric constant varies approximately from 3-5[21]. We

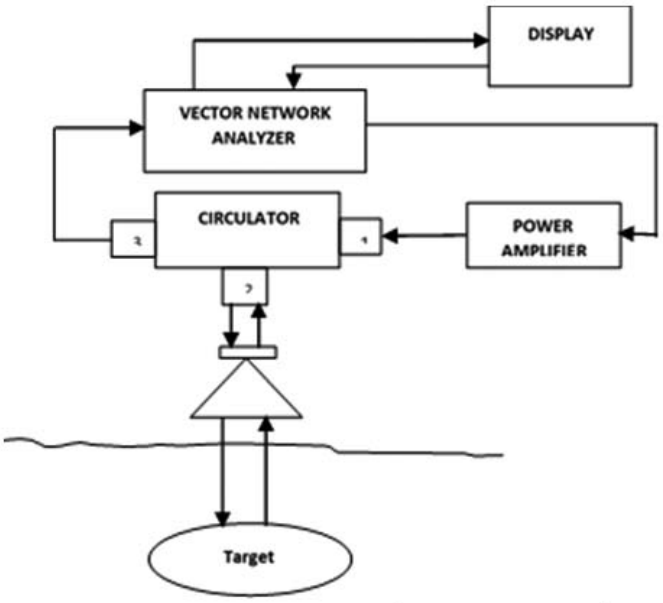

Figure 1. Monostatic ground penetrating radar system[23].

have considered the average soil dielectric constant 4. If the medium has a relative dielectric constant then range resolution for SFCW GPR is as given by following Eqn. (22)

$$\Delta R = \frac{c}{2N\Delta f\sqrt{\epsilon_r}} \tag{1}$$

where is the velocity of light = $3x10^8$ m/s

N is the number of frequency points = 631

Δf is the frequency interval between successive frequency points = 1.58 MHz (from Table 1)

ϵ_r is the relative dielectric constant of medium = 4

ΔR is the range resolution

$$= 3x10^8 / 2\ x631x1.58\ x10^6\sqrt{4} = 7.52x10^{-2}\ m = 7.52\ cm$$

When dealing with GPR images, there are several different types of 'scans'. The simple GPR range profile is known as A-scan[24], which is as shown in Fig. 2. In Fig. 2, three A-scan profiles like profile with target, profile without target and

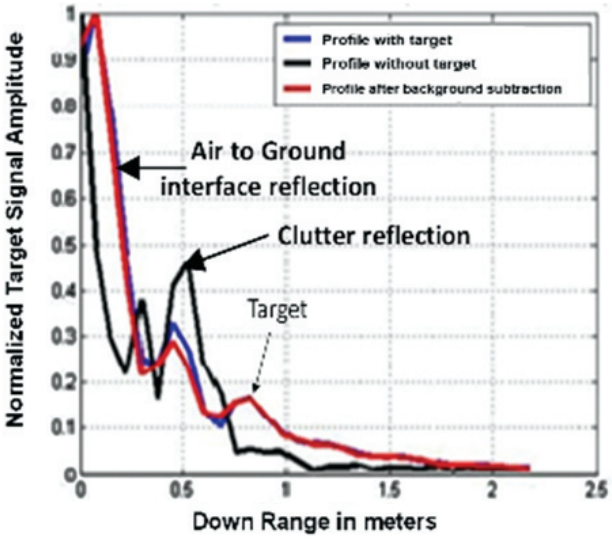

Figure 2. A scan range profile with target-1 (Dataset$_{21}$) and without target and after background subtraction.

profile with background subtraction are shown with a number of reflection peaks[23]. As seen from A-scan profiles, clutter peaks behave like a target in without target A-scan profile, even after background subtraction techniques have been applied. This criticality shows the necessity of the development of efficient methodology to separate out the background and foreground signals.

Table 1. Experiment details with (a) specifications of GPR system (b) field observations for practical readings and (c) targets descriptions for GPR system

GPR active radar parameter	Typical Value
Operating frequency	1 GHz-2 GHz
No. of frequency points (N)	631
Transmitted power	1 mW
Antenna type	Double Ridge Horn Antenna
Range resolution	15 cm
Antenna height from ground	15 cm
Investigated depth	≤ 1 m
No. of cross range points	20
Frequency step size ($\Delta f0$)	1.58 MHz

(a)

Field observations parameter	Typical Value
Soil Moisture of ground	5-15 % in 5 % interval, GND1 = 5 %, GND2 = 10 % and GND3 = 15%
Depth of targets inside ground with soilmoisture content	15 cm - 50 cm in 5 cm interval and each depth dataset measured with 5 %, 10 % and 15 % of soil moisture e.g. (Target-1, $Dataset_{13}$) = 35 cm depth and 10 % soil moisture

(b)

Targets used for GPR system	Targets description
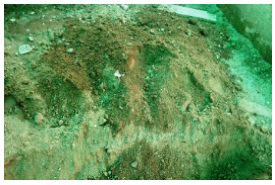	Ground Ground field area for experiment with soil moisture variation at IIT, Roorkee (Results are as shown only for GND3 ground data)
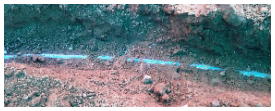	Target-1 Type: Long PVC Pipe Material: PVC Dimension : (300 cm x 5 cm)
	Target-2 Type: Small PVC Pipe Material: PVC Dimension : (150 cm x 5 cm)
	Target-3 Type: Mine Material: Plastic Dimension : (Height x Diameter =7 cm x 25 cm)
	Target-4 Type: Water Bottle Material: Thin PVC Dimension : (40 cm x 10 cm)

(c)

*Results are shown only for target-j $Dataset_{21}$=35 cm depth and 15 % soil moisture, where j= 1,2,3,4.
*In Table 1, collected data have been denoted by (targets, $Dataset'_i$).
*Targets may be ground, target-1 (i.e Long PVC pipe), target-2 (i.e. Small PVC pipe), target-3 (i.e. Mine) and target-4 (i.e. Water bottle).
*$Dataset'_i$ denotes collected data for corresponding target, where subscript i represents the collected data number for particular depth and moisture.

Usually, GPR data processing is based on a collection of a number of A-scans. It forms a 2D matrix for creating GPR images for the area of interest and is known as B-scan. More than thousands of data were collected with buried target and without buried target (i.e., ground only) in various field conditions with 5-15 per cent moisture variation. The field was prepared for the specified moisture level with the help of a moisture meter for collecting the data at a variety of locations. Table 1 shows the considered four targets, where 24 datasets for each target have been collected with 15-50 cm buried target depth varies in 5 cm interval of 5 %, 10 %, and 15 % soil moisture, i.e. for each depth there are 3 datasets. There are total 96 measured datasets for four targets and 3 datasets for ground. Each target dataset has been validated with burial depth and soil moisture, but in results only target $dataset_{21}$ has been considered.

The main problem with the collected data was how to separate background and foreground data in the presence of soil moisture and clutters due to ground non-linearity. The proposed algorithm may resolve the stated problem, which will be discussed in subsequent sections.

3. THEORETICAL BACKGROUND

The thresholding is mainly a function of mean and variance of the image data. The image is segmented into two parts by taking a function of the mean and standard deviation as initial threshold and the values below this threshold is considered as background image and the values above as foreground image. The function can be changed as per the needs and uses. A proper trade-off is needed to be derived for proper imaging in GPR as well as in other methods. A higher threshold may lead to the exclusion of important details and even prevent detection, while a lower threshold would lead to inclusion of noise and may lead to clutter effects. As per above considerations, the thresholding of an image can be classified in following ways:

- Otsu's Method[7]: The Otsu's method is based on variances, which are derived from the probability theory. The procedure starts by defining the global mean.
- Recursive Thresholding Technique[7]: The recursive thresholding technique involves the iterative computation to compute the threshold value for an image.

- Adaptive Progressive Thresholding (APT)[7]: This algorithm makes use of both Otsu's technique and the recursive method.

These methods are very popular and generalised image processing applications, but GPR images are contaminated by clutters as shown in Fig. 3.

In Fig. 3(a) - 3(b), considered targets are ground and mine, which are as shown in the Table 1. There are only clutter components with a maximum strength of 0.7 index in Fig. 3 (a) for ground data (Ground, Gnd3), but in Fig. 3(b), for mine target data (target-3, Dataset$_{21}$), the clutter components are mixed with non-metallic target components (i.e. Mine) with a maximum strength of 0.7 index. Here, the index represents the pixel intensity for clutter and target, and the intensity scales may vary for ground and for non-metallic targets. Therefore, it cannot be determined as to 'which components are clutter components and which target components are'. The main aim of this paper is to separate the clutter and target information. In the next section, an adaptive thresholding algorithm has been proposed to achieve the said objectives.

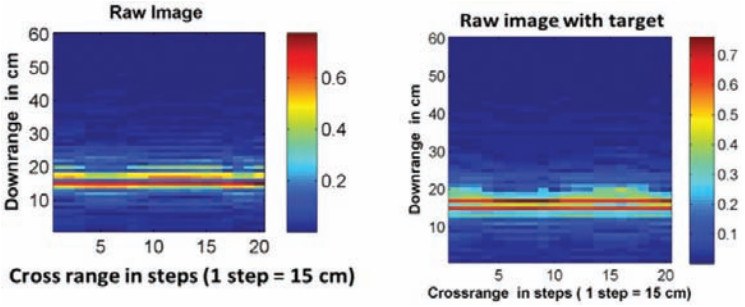

Figure 3. (a) Raw image of ground for dataset (Gnd3) and (b) Raw image of buried mine data (Dataset$_{21}$).

3.1 Proposed Adaptive Threshold Algorithm

In many applications of image processing, the intensity of the object pixels are quite different from the intensity of the background pixels. Thresholding is a simple but effective method to separate objects from the background. From GPR perspective, buried object information pixel's intensity should be different from the pixel intensity belonging to clutter or background. The proposed algorithm is based on variance ratio estimation of buried non-metallic or metallic object, which decides the lower and upper threshold with polynomial curve fitting. Due to ground variation, an increase in failing to detect present target (type II error) results, which may either, be a false positive target or false negative target. Another aspect is that improper selection of the threshold may enhance the false positive and false negative target problems. So, the variance may play a major role is to minimising these false positive and false negative target detection problems. To solve these problems, a variance ratio based approach is proposed, which estimates the lower and upper threshold adaptively for actual GPR measurement with reference to normal distributed random data.

The raw GPR data are in frequency domain B-scan M×N data matrix. This frequency domain data matrix is converted into the time domain data matrix, which is also M×N using inverse Fourier transform, where M is sample point and N is the cross range position. Further, to reduce the additive noise, windowing is applied.

Pre-processed data have been obtained from Fig. 4 for further post-processing. In terms of random variable, the proposed algorithm methodology can be mathematically derived.

Let X be the normal distributed random variable with MxN dimension. σ^2_{rand} be the variance of X.

$$\sigma^2_{rand} = \left[\sigma^2_1, \sigma^2_2, \sigma^2_3 \ldots..\sigma^2_N\right]^T,\ Nx1 \tag{2}$$

where $var(X) = E\left[\left(X - \bar{X}\right)^2\right]$, $\bar{X}$ *is the mean of* X

Equation (2) represents the estimated clutter/noise vector, when consider in GPR measurement asnormally-distributed[13].

Minimum variance[13] of X is calculated using the following equation:

$$\sigma^2_{randmin} = \frac{1}{\sum_{i=1}^{N} \frac{1}{\sigma^2_i}} \qquad i = 1, 2\ldots.., N \tag{3}$$

where $\sigma^2_{randmin}$ denotes the minimum noise level of random variable X. Now, for random variable X, the variance ratio[19] for N independent observations are

$$T_{rand} = \sigma^2_{irand} \Big/ \sigma^2_{randmin} \qquad irand = 1, 2, \ldots\ldots.., N \tag{4}$$

where T_{rand} is random variable ratio, σ^2_{irand} is obtained from Eqn. (2) and $\sigma^2_{randmin}$ is obtained from Eqn. (3). Physically Eqn. (4) estimates the clutter content in the GPR image.

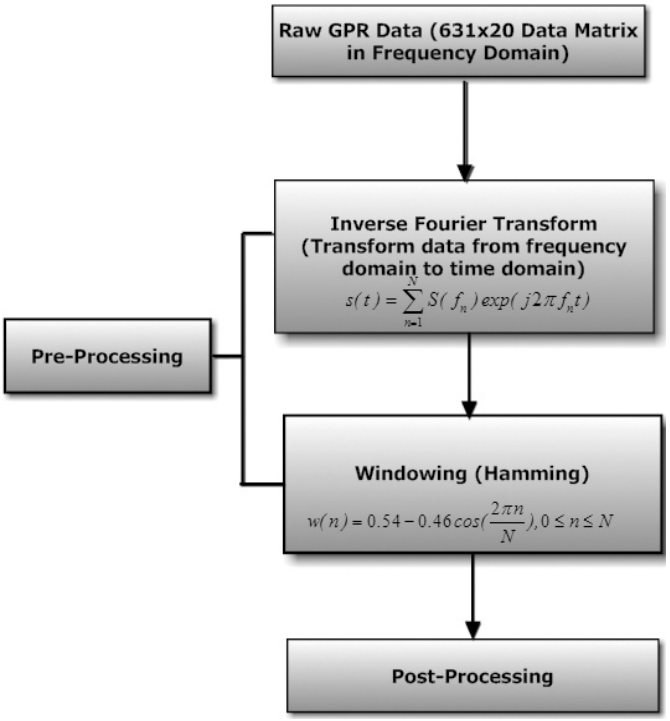

Figure 4. Flowchart of GPR signal processing[23].

3.2 Clutter and Foreground Separation for GPR Data

Consider GPR measurement with N observations in the area of interest. Each measurement is corrupted by a variety of noise levels. Let $y_1, y_2, y_3, \ldots\ldots, y_n$ be the true GPR signal, that have to be estimated and $d_1, d_2, d_3, \ldots\ldots, d_n$ denotes the noise vector for N observations. The GPR measurement model equation is

$$S = Ay + d \tag{5}$$

where $S = (s_1, s_2, s_3, \ldots\ldots, s_n)^T$ is an N observation vector A is a constant vector and $d = (d_1, d_2, d_3, \ldots\ldots, d_n)^T$ is an observation noise. In general scenario, observation noise follows a normal distribution, then from the Eqn. (2)

$$\sigma_d^2 = \sigma_{rand}^2 \tag{6}$$

where σ_d^2 is the observation variance.

But,GPR measurement does not follow the normal distribution due to the non-Gaussian process, so

$$\sigma_d^2 \neq \sigma_{rand}^2 \tag{7}$$

If σ_S^2 is the variance of actual GPR measurement, then variance is

$$\sigma_S^2 = \left[\sigma_{S1}^2, \sigma_{S2}^2, \sigma_{S3}^2 \ldots..\sigma_{SN}^2\right]^T,\ Nx1 \tag{8}$$

Minimum variance[13] of GPR measurement from the Eqn. (3) is

$$\sigma_{Smin}^2 = \frac{1}{\sum_{i=1}^{N} \frac{1}{\sigma_{Si}^2}} \qquad i = 1, 2 \ldots.., N \tag{9}$$

where σ_{Smin}^2 is GPR measurement, minimum variance.

Variance ratio[19] for GPR measurement is obtained from the Eqn. (4) as

$$T_S = \sigma_{Si}^2 \Big/ \sigma_{Smin}^2 \qquad i = 1, 2, \ldots\ldots.., N \tag{10}$$

Equation (10) represents the actual measured clutter content with respect to minimum clutter content.

To separate out foreground and background, there is a need to derive the threshold level from the estimated clutter/ noise contents.

Let Th_1 denote upper threshold value, then lower threshold value can be estimated by Eqn. (11).

$$Th_2 = \frac{Th_1}{N_1} \tag{11}$$

where Th_2 denotes lower threshold value, which is derived from upper threshold value and N_1 is scaling factor for lower threshold.

To separate the clutter and foreground, apply threshold limit

$$\left\{\begin{array}{l} If \quad T_S \leq Th_2 \rightarrow \quad Clutter \\ If\ Th_2 < T_S \leq Th_1 \rightarrow Foreground \end{array}\right\} \tag{12}$$

Once Th_1 and Th_2 are decided then, clutter and foreground can be easily distinguished.

3.3 Optimum Threshold Decision

The lower threshold value Th_2 and the upper threshold value Th_1 can be estimated by Eqns. (11) and (12), respectively. The problem, however, in both threshold values is to determine their optimum values. As seen from Eqns. (11) and (12), both threshold values depend on the value of N_1. Therefore, inherently optimum value of N_1 will play an important role in deciding the optimum value of thresholds. To solve the problem, curve intersection approach has been applied. The linear model of n[th] order polynomial is

$$p(x) = p_1 x^n + p_2 x^{n-1} + p_3 x^{n-2} + \ldots\ldots\ldots + p_{n+1} \tag{13}$$

where $p(x)$ is nth order polynomial, $p_1, p_2, \ldots\ldots\ldots, p_{n+1}$ are polynomial coefficient and is input row vector.

In polynomial curve fitting, data has been fitted with corresponding data in least square sense.

From Eqn. (8)

$$x = N_i * \sigma_{Si}^2 \quad i = 1, 2, 3, \ldots\ldots\ldots.. \tag{14}$$

In the present case, linear curve fitting for Table 2 data is represented by the Eqn. (15).

$$f_1(x) = p_1 x + p_2 \tag{15}$$

where $RMSE = 0.0046$, *Root mean square error*

Similarly, 6[th] order polynomial fitting for Table 2 data is represented by the Eqn. (16):

$$f_2(x) = p_1 x^6 + p_2 x^5 + p_3 x^4 + p_4 x^3 + p_5 x^2 + p_6 x + p_7 \tag{16}$$

where Error! Objects cannot be created from editing field codes.

Table 2. Data for Polynomial Fitting

Scaled measured clutter $x = N_i * \sigma_{Si}^2$ **(X-axis)**	**Estimated clutter using synthetic data** $T_{rand} = \sigma_{irand}^2 \Big/ \sigma_{randmin}^2$ **(Y-axis)**
0.366490839267332	0.440619108731061
0.665989625308906	0.440320663274159
1.17037613931152	0.439923517696339
1.34555140554018	0.447965349600226
1.66260931286166	0.436473819423967
2.24897461148112	0.440887498039732
2.41719315040346	0.441894842825221
3.00962163409210	0.433889507168937
3.09106289900514	0.436075574406000
3.76911762942385	0.448879095321608
4.13501630723191	0.440930269806022
4.47137540416587	0.452551804095571
4.91633552811514	0.443708208132163
5.62238600045579	0.451833401861123
5.54150053097929	0.447160591926667
5.29253801194672	0.442633185203154
6.59357060862760	0.454022745320899
5.85730792385215	0.449338450747496
6.40990756478422	0.450643657360696
6.78706816233295	0.451708768263113

Intersection Point can be obtained by the Eqn. (17).

$$\left(f_1(x) - f_2(x)\right) < RMSE \tag{17}$$

Corresponding data for fitting is obtained from the Eqn. (4), which is the variance ratio of random data. The polynomial fitting for 6th order is applied to the Eqn. (16) and for linear way, i.e. the 1st order is applied to the Eqn. (15). X-axis data in Table 2 are scaled measured clutter/noise and Y-axis data are estimated clutter/ noise for synthetic data as from Eqn. (4) in least square sense and it is observed that both the fitted data intersect with each other according Eqn. (17) conditions. Statistics of 6th order polynomial fitting and of 1st order polynomial fitting i.e. linear fitting are as shown in Table 2. Coordinates of intersected points provide the upper threshold value on Y-axis and the lower threshold value scaling factor on the X-axis. If more than one intersection point occurs, then the maximum value of intersect point will be taken as threshold coordinate, because maximum value will take care all clutter/ noise levels. From Fig. 5, maximum values intersection points for linear fitting and for 6th order polynomial fitting provide the value of optimum upper threshold value on Y-axis and optimum scaling factor value on X-axis for optimum lower threshold value, where X-axis denotes the measured scaled clutters and Y-axis denotes the estimated clutter.

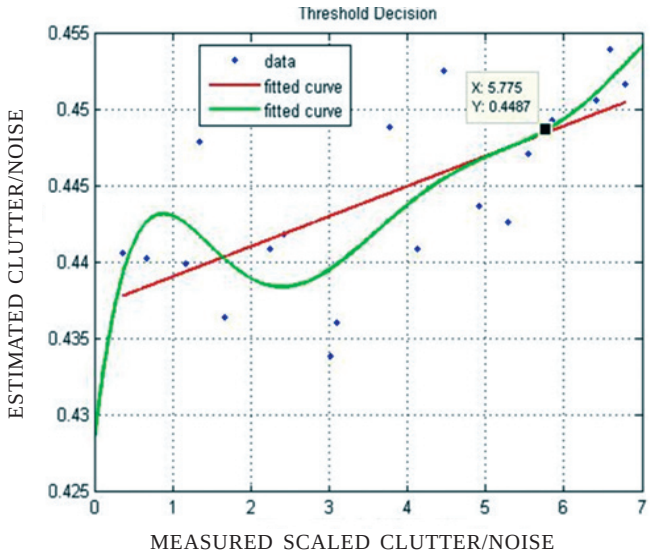

Figure 5. Optimal threshold detection using intersection of polynomial and linear curve fitting.

3.4 Data Smoothening

In GPR measurements the data is corrupted by noise and clutter like Gaussian noise, non-Gaussian noise, surface variation effects and moisture. The data smoothening, which is used to reduce these unwanted effects and equalize the background intensity, may help to enhance the target characteristics. Therefore, after optimum threshold decision from Fig. 5, clutter and foreground are separated out. Example of thresholded and data smoothened images of small PVC pipe target from Table 1 are shown in Figs. 6(a)-6(b) for small PVC data (target-2, $Dataset_{21}$). From Fig. 6(a) it is still difficult to visualize the target, therefore, Data smoothening has been applied, which has been derived as follows:

Let X_{raw} be the GPR measured data in time domain with MxN dimensions, where M denotes number of measured data points and N denotes number of observations. From Eqn. (12)

$$Data_{smooth} = T_{si} \le Th_2 \quad i = 1,2,,3,...,N \tag{18}$$

$$S_{smooth} = \sum_{i=1}^{N} Data_{Smoothi} \Big/ N \quad i = 1,2,3,\ldots N \tag{19}$$

where $Data_{smooth}$ represents background data in presence of target data and denotes the smoothing factor, which equalises the background.

Final smoothed output data is

$$X_{out} = S_{smooth} * X_{fore} \tag{20}$$

where X_{out} represents final smoothed output data with equalised background intensity and X_{fore} denotes target information data (i.e. Foreground) after thresholding. After getting smoothed data, target signature can easily be detected, which is as shown in Fig. 6(b) for small PVC pipe (target-2, $Dataset_{21}$).

The algorithm steps can be summarised as follows:

1. X be the normal distributed random variable with MxN dimensions. σ^2_{rand} be the variance of X
2. $\sigma^2_{randmin} = \dfrac{1}{\sum_{i=1}^{N} \dfrac{1}{\sigma_i^2}}$, $i = 1,2\ldots..,N$, is represents the synthetic data minimum variance.
3. $T_{rand} = \sigma^2_{irand} \Big/ \sigma^2_{randmin}$ $irand = 1,2,\ldots\ldots..,\ N,$ Representing the synthetic data variance ratio for the estimation of value of upper threshold.
4. $S = Ay + d$ where y istrue GPR signal vector and d is noise/clutter
5. $\sigma_d^2 = \sigma_{rand}^2$ where σ_d^2 represents the noise/clutter variance. This condition can be satisfied, if measured data will follow the normal distribution.
6. $\sigma_d^2 \neq \sigma_{rand}^2$, in actual, GPR noise/clutter does not follow the normal distribution.
7. σ_S^2 is the variance of actual GPR measurement , which represents the overall noise/clutter variance.
8. $\sigma^2_{Smin} = \dfrac{1}{\sum_{i=1}^{N} \dfrac{1}{\sigma^2_{Si}}}$ $i = 1,2\ldots..,N$ where σ^2_{Smin} GPR measurement, minimum variance.
9. $T_S = \sigma^2_{Si} \Big/ \sigma^2_{Smin}$ $i = 1,2,\ldots\ldots..,N$ is the variance ratio of actual GPR measurement, which is used to decide, whether GPR data is clutter or foreground.
10. $p(x) = p_1 x^n + p_2 x^{n-1} + p_3 x^{n-2} + \ \ldots\ldots\ldots + p_{n+1}$ polynomial curve fitting is applied to select the scaling factor N_1 for lower threshold.
11. 1st order and 6thorder polynomial curve fitting for $R^2 > 0.8$ are intersected with each other.
12. The intersection point is obtained by $\left(f_1(x) - f_2(x)\right) < RMSE$
13. If multiple RMSE values are obtained, the minimum RMSE will be considered for finding the intersection points.

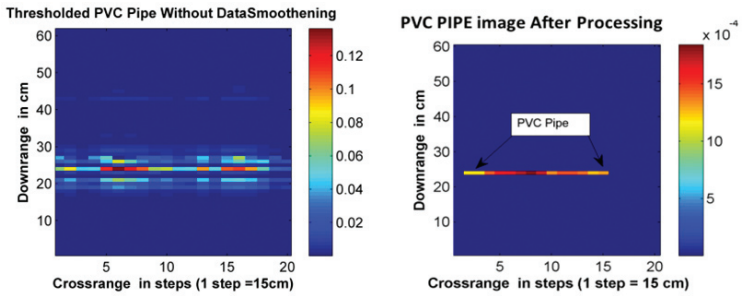

Figure 6. (a) Thresholdeds mall PVC pipe image for target-2(Dataset21) without data smoothening and (b) Image of small PVC pipe for target-2 (Dataset$_{21}$) after data smoothening.

14. Maximum value of intersection point has been considered for multiple intersect points.
15. The y-axis value of intersection point gives the upper threshold value (Th_1) and X-Axis value gives scaling factor for lower threshold ($Th_2 = \frac{Th_1}{N_1}$).

$$\begin{Bmatrix} If \quad T_S \le Th_2 \rightarrow \quad Clutter \\ If\ Th_2 < T_S \le Th_1 \rightarrow Foreground \end{Bmatrix}$$

16. $x = N * \sigma^2_{Si} \qquad i = 1,2,3,\ldots\ldots\ldots..N$ is scaled actual measured noise/clutter.
17. $Data_{smooth} = T_{si} \le Th_2 \qquad i = 1,2,,3,\ldots\ldots\ldots..,N$ represent N number of clutter data.
18. $S_{smooth} = \sum_{i=1}^{N} Data_{Smoothi} / N \qquad i = 1,2,3,\ldots\ldots\ldots N$ represent the average value of data smoothening factor.
19. $X_{out} = S_{smooth} * X_{fore}$ where X_{out} represents final smoothed output data with equalised background intensity and X_{fore} denotes target information data (i.e. Foreground) after thresholding.

4. RESULTS AND DISCUSSIONS

The proposed algorithm in section 3 has been as shown in the flow chart in Fig. 7. There is an input GPR data matrix of MxN dimension, where M represents the number of frequency points at one observation point and represents a number of observation points. In the present case, value of M is 631 and value N is 20. Similarly, another synthetic normally distributed data matrix of MxN dimension has been generated to estimate the lower and upper threshold values, respectively.

Unprocessed GPR data matrix images for clutter (i.e., ground only) and target are as shown in Figs. 8(a) - 8(b). In these figures highest colour intensity represents the target signature, but both images have highest intensity components. Therefore, it cannot be decided that either Figs. 8 (a) - 8(b) contains target components or not. Due to this reason, variance ratio has been calculated from Eqns.(3) and (9) for synthetic data and for actual GPR measurement of Fig. 8(a) and 8(b) respectively. The upper threshold value and the lower threshold value are unknown parameters. To calculate the both threshold values, curve intersection technique has been used, where 6th order polynomial ($R^2 > 0.8$) has been used for curve intersection with a linear curve for the same data. As shown in Fig. 5, X-axis represents the Eqn. (13), where target signal variance σ^2_S with scaling of N sweep. On the Y-axis random signal variance ratio as from the Eqn. (3) has been represented. The upper threshold value may be obtained from the maximum intersected value of both curves on Y-axis, which is found at 0.452 from Fig. 5. Similarly, the scaling factor for the lower threshold value may be obtained as the projection from the maximum linear region of the fitted curve to X-axis. Therefore, the scaling factor value is found to be ~6.588 as from Fig. 5 and the lower threshold value is 0.0684.

As seen from Fig. 7, if the variance ratio T_S for actual GPR measurement is less than or equal to the lower value (0.0684), it can be declared that measured data has no target information, i.e. only clutter. On the other hand, if variance ratio T_S for actual GPR measurement is greater than the lower threshold value (0.0684) and less than or equal to the

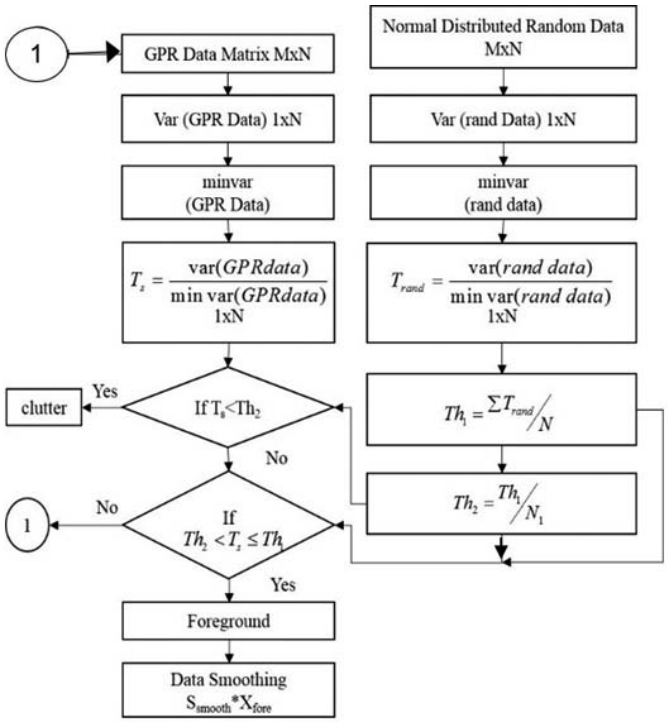

Figure 7. Implementation of adaptive threshold and data smoothening algorithm.

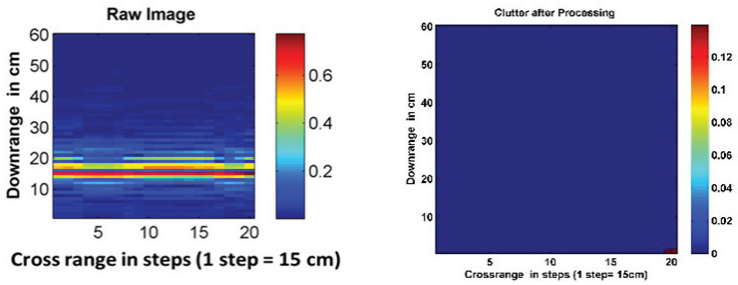

Figure 8. Results of developed adaptive thresholding and data smoothening (a) Raw image of Clutter for ground data (Gnd-3) and (b) Processed image of clutter after Thresholding for ground data (Gnd-3).

upper threshold value (0.452), then measured data has target information, i.e., foreground. If both these conditions are not satisfied, then the same process will be repeated for the next measurement. Once, it decides that measured data has target information (i.e., foreground) then further data smoothing process will be started. The data smoothing factor can be calculated by Eqns. (13) and (18). In present scenario, the data smoothing factor S_{smooth} value is 0.0279, which is multiplied by X_{fore} (Target information data) to equalise the background intensity and get the stable target information.

The proposed algorithm has been experimentally applied to various buried objects and results are as shown in Figs. 9 - 12. The considered targets are as shown in Table 1 and experimentally collected data have been denoted by (targets, Dataset'$_i$). Where targets are ground, target-1 (i.e. Long PVC pipe), target-2 (i.e. Small PVC pipe), target-3 (i.e. mine) and target-4 (i.e. Thin Plastic bottle). The Dataset'$_i$(where subscript i represents number of collected data of a target) are denoted the collected data for corresponding depth's and moistures which is as shown in Table 1. Analyses of resultant images of various buried objects are the following:

In Figs. 8(a) - 8(b), considered ground as target with ground data (GND3), which is as shown in Table 1. The unprocessed clutter data (i.e. only ground data) has some target like components, denoted by dark brown colour. After applying blind thresholding and data smoothing (from Fig. 7), the lower threshold of 0.1233 and the upper threshold of 0.7829 are obtained. These threshold values totally remove the clutter and only clean ground data is left, which is denoted by blue colour.

In Figs. 9(a) - 9(b), the considered target is long PVC pipe (target-1, Dataset$_{21}$) from Table 1, i.e. long PVC pipe, which is buried at 35 cm depth with 15 per cent moisture and the data covers whole measurement cross range steps, i.e. from the start point of measurement to stop point of measurement. The unprocessed image shows a dark brown line with clutter components. There is no evidence to say whether "PVC pipe is buried or not" Because the detected line may be corresponded to clutter. Therefore, the unprocessed image is analysed by the proposed adaptive threshold algorithm as shown in Fig. 7, to get 0.1263 as lower threshold and 0.884 as upper threshold. With these threshold values for long PVC pipe a stable and smooth image for long PVC pipe is obtained, as shown in Fig. 9(b).

In Figs. 9(a) - 9(b), the long PVC pipe is laid in whole cross range. Due to this, there is no discrimination possible between unprocessed image and blind thresholded image. Therefore, a small PVC pipe is considered as the target to validate the long PVC Pipe result, which is not covered in the whole cross range (i.e. Total GPR measurements). From Table 1, the results for small PVC pipe (target-2, Dataset$_{21}$) data are as shown in Figs. 10(a) - 10(b). As seen from Fig. 10(a), there is no information from the unprocessed image to decide whether the small PVC pipe has been detected or not. Since the whole cross range points are showing a dark brown line, it may or may not be a small PVC pipe. Further, after applying the blind threshold algorithm (Fig. 7), again we get the lower and upper threshold values, which are 0.1297 and 0.9078, respectively. The thresholded small PVC pipe image is as shown in Fig. 10(b).

GPR can also be used to detect land mines. To check the blind threshold algorithm applicability on buried mine as a target, from Table 1 for (target-3, Dataset$_{21}$), the results obtained with a mine are as shown in Fig. 11 (a)-(b). There is only clutter visualised (i.e. Two dark brown lines) in the unprocessed image as seen from Fig. 11(a). The mine signature has come out after applying adaptive threshold algorithm or blind threshold (from Fig. 7) on the unprocessed image of mine, which is as shown in Fig. 11(b). In this case, lower threshold and upper threshold values are 0.1312 and 0.7922, respectively.

From Table 1, the results for thin plastic water bottle data (target-4, Dataset$_{21}$) are as shown in Figs. 12(a) - 12(b). There

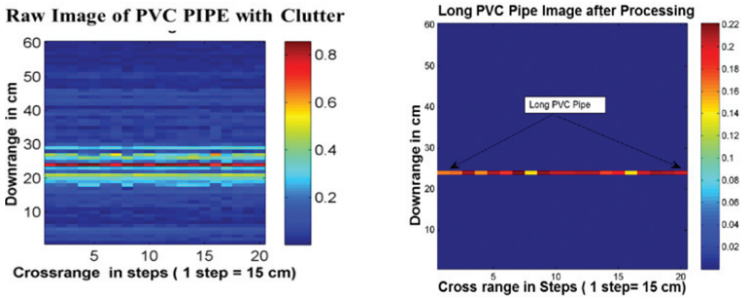

Figure 9. (a) Raw image of Long PVC Pipe data (target-1, Dataset$_{21}$) and (b) Processed image of Long PVC Pipe after Thresholding (target-1, Dataset$_{21}$).

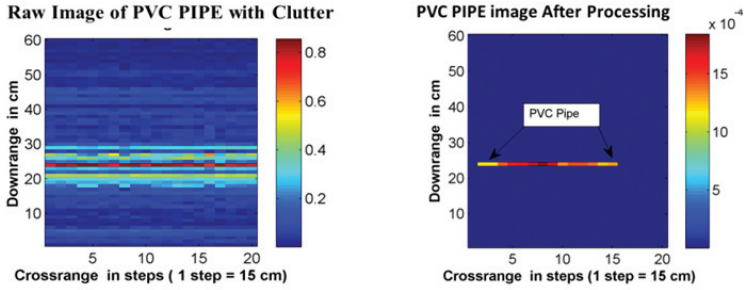

Figure 10. (a) Raw image of small PVC Pipe data (target-2, Dataset$_{21}$) and (b) Processed image of small PVC pipe data after Thresholding (target-2, Dataset$_{21}$).

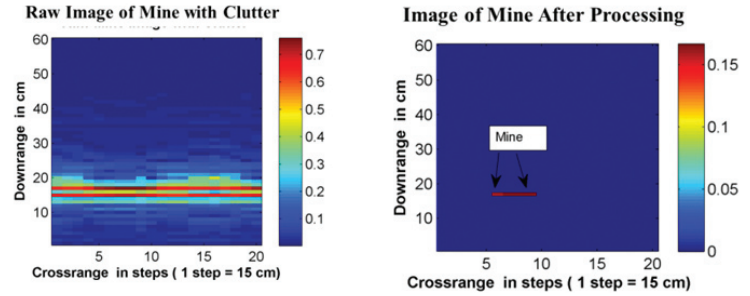

Figure 11. (a) Raw image of mine data (target-3, Dataset21) and (b) Processed image of mine after Thresholding (target-3, Dataset$_{21}$).

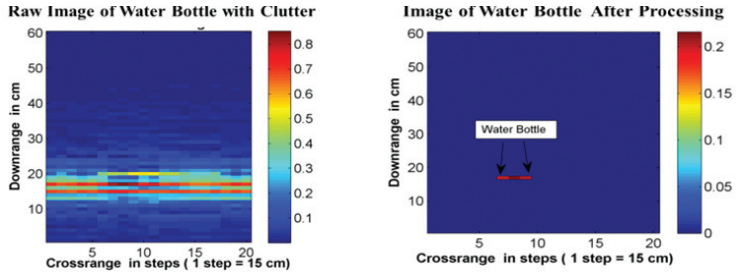

Figure 12. (a) Raw image of water bottle data (target-4, Dataset$_{21}$) and (b) Processed image of water bottle after thresholding (target-4, Dataset$_{21}$).

is no information about the water bottle from Fig. 12(a). Using the proposed adaptive threshold algorithm as shown in Fig. 7, the pixels, corresponding to water bottle are obtained (shown in Fig. 12(b)). The calculated lower and upper threshold values for water bottle are 0.1233 and 0.8631 respectively.

The developed algorithm can detect various material underground targets as well as distinguish the background and foreground. The algorithm has the advantage of generating the auto threshold value without reference data. Therefore, the proposed algorithm has equal applicability in other image processing applications, where threshold value is unknown.

5. CONCLUSIONS AND FUTURE WORK

In this paper, a blind threshold problem has been attempted for GPR applications. When the threshold reference value is not known, thresholding becomes a difficult task. The proposed blind threshold and data smoothening algorithm successfully separates the background, foreground and smoothens the data with the help of statistical analysis of random data and actual measured data. Statistical analysis helps to select the various parameters for implementing the algorithm. In GPR, threshold values change from surface to surface, due to soil moisture and surface roughness. Therefore, the algorithm has included a lower threshold and upper threshold, which is based on normal distributed random data. After thresholding, some clutter components may remain, which can be filtered out by using data smoothing factor. Proposed algorithm has been tested on various buried targets (e.g. PVC pipes, mine, thin plastic water bottle etc.). All targets have been detected with clutter free images by blind threshold algorithm. Future work is to incorporate the classification of detected targets and shape identification of detected targets.

REFERENCES

1. Israr, H. & Hujun, Y. A novel wavelet thresholding method for adaptive image denoising. ISCCSP, Malta, 12-14 March 2008, 1252-1256. doi: 10.1109/ISCCSP.2008.4537418
2. Said, G. The use of wavelet-based denoising techniques to enhance the first-arrival picking on seismic traces.*IEEE Trans.Geosci. Remote Sensing*, 2014, **52**(8), 4558-4563. doi: 10.1109/TGRS.2013.2282422
3. Yijun, S. & Jian, L. Adaptive learning approach to landmine detection. *IEEE Trans. Aerospace Electronic Sys.*,2013, **41**(3), 1-10. doi: 10.1109/TAES.2005.1541442
4. Abdolhossein, F. & Ahmad, R. N.N. Efficient image denoising method based on a new adaptive wavelet packet thresholding function. *IEEE Trans. Image Processing*, 2012, **21**(9), 3981-3990. doi: 10.1109/TIP.2012.2200491
5. Farshad, F. & Michael, S. Combining spatial and scale-space techniques for edge detection to provide a spatially adaptive wavelet-based noise filtering algorithm. *IEEE Trans. Image Processing*, 2002, **11**(9), 1062-1071. doi: 10.1109/TIP.2002.802526
6. Florian, L.; Thierry, B. & Michael, U. Image denoising in mixed poisson–gaussian noise. *IEEE Trans. Image Processing*, 2011, **20**(3), 696-708. doi: 10.1109/TIP.2010.2073477
7. Valaparla, D.P. & Vijayan K.A. An adaptive technique for the extraction of object region and boundary from images with complex environment. *In* IEEE Applied Imagery Pattern Recognition Workshop, 2001, 194-199. doi: 10.1109/AIPR.2001.991226
8. Torrione, P.A.; Chandra, S.T. & Leslie, M.C. Performance of an adaptive feature-based processor for a wideband ground penetrating radar system. *IEEE Trans. Aerospace Electronic Syst*., 2006, **42**(2), 644-658. doi: 10.1109/TAES.2006.1642579
9. Rais, N.B.; Hanif, M.S.&Imtiaz, A.T. Adaptive thresholding technique for document image analysis. *In* 8th International IEEE Proceedings on Multitopic Conference, INMIC 2004, 61-66. doi: 10.1109/INMIC.2004.1492847
10. Francis, H.Y.C.; F. K.L. & Hui Z. Adaptive thresholding by variational method. *IEEE Trans. Image Processing*, 1998, **7**(3), 468-473. doi: 10.1109/83.661196
11. Fei, L.; Xiao, D. S.; Yupin, L. & Dongcheng, H. Adaptive thresholding based on variational background. *Electronics Letters*, 2002, **38**(18), 1017-1018. doi: 10.1049/el:20020728
12. Vladimir P.M.; Ilya S.; Karen E. & Jaakko A. Block-Median pyramidal transform: Analysis and denoising applications. *IEEE Trans. Signal Processing*, 2001, **49**(2), 364-372. doi: 10.1109/78.902119
13. Shesheng, G.; Yongmin, Z. & Wei, L. Random weighting method for multisensor data fusion. *IEEE Sensor Journal*, 2011, **11**(9), 1955-1961. doi: 10.1109/JSEN.2011.2107896
14. Zhang, Y.; Panglijen, C.; Guoan, W. & Tian, X. 2-D entropy and short-time Fourier transform to leverage GPR data analysis efficiency. *IEEE Trans. Instrumentation Measurement*, 2015, **64**(1), 103-111. doi: 10.1109/TIM.2014.2331429
15. Peng, W.; Xu, H. & Xie, P. Research on ground penetrating radar image denoising using nonsubsampled contourlet transform and adaptive threshold algorithm. *Int. J. Signal Processing, Image Processing Pattern Recognition*, 2016, **9**(5), 219-228.

doi: 10.14257/ijsip.2016.9.5.19

16. Nabelek, D. & Ho, K.C. Detection of deeply buried non-metal objects by ground penetrating radar using non-negative matrix factorization. *In* SPIE Defense+ Security, International Society for Optics and Photonics, 2015, 945419-945419.
doi: 10.1117/12.2177481
17. Abeynayake, C. & Minh D. T. Automatic target detection and discrimination algorithm applicable to ground penetrating radar data. *In* Detection and Sensing of Mines, Explosive Objects, and Obscured Targets XX, International Society for Optics and Photonics, 2015, **9454**, p. 945411.
doi: 10.1117/12.2087297
18. Zhang, Y.; Anbu, S. V.; Dryver, H. & Tian, X. Advanced signal processing method for ground penetrating radar feature detection and enhancement. *In* Proc. SPIE, 2014, **9063**, p. 906318.
doi: 10.1117/12.2046338
19. Kalika, D.; Mary, T. K.; Leslie, M.C.; Peter A.T. & Kenneth, D.M. Leveraging robust principal component analysis to detect buried explosive threats in handheld ground-penetrating radar data. *In* SPIE Defense+ Security, International Society for Optics and Photonics, 2015, 94541D.
doi: 10.1117/12.2177944
20. Morton, K.D.; Leslie, M.C. & Peter, A.T. A robust bayesian approach to target detection applied to explosive threat detection in handheld ground penetrating radar data. *In* SPIE Defense+ Security, International Society for Optics and Photonics, 2014,90720R.
doi: 10.1117/12.2050514
21. Tiwari, K.C.; Dharmendra S. & Manoj K. A. Development of a model for detection and estimation of depth of shallow buried non-metallic landmine at microwave X-band frequency. *In* Progress in Electromagnetics Research, 2008, **79**, 225-250.
doi:10.2528/PIER07100201
22. Yamaguchi, Y.; Yasuichi M.; Atsushi K.; Masakazu S. & Takeo A. Detection of objects buried in wet snowpack by an FM-CW radar.*IEEE Trans. Geoscience Remote Sensing*, 1991, **29**(2), 201-208.
doi: 10.1109/36.73660
23. Sharma, P.; Kumar, B.; Singh, D. & Gaba, S.P. Critical analysis of background subtraction techniques on real GPR Data. *Def. Sci. J.*, 2017, **67**(5), 559-571
doi: 10.14429/dsj.67.10048
24. Sharma, P.; Kumar, B.; Singh, D. & Gaba, S.P. Non-metallic pipe detection using SF-GPR: A new approach using neural network. *In* IEEE Geoscience and Remote Sensing Symposium (IGARSS) 2016.
doi: 10.1109/IGARSS.2016.7730726

ACKNOWLEDGMENTS

The author would like to express his special gratitude to Shri Benjamin Lionel, Director, Instrument Research and Development Establishment, Dehradun, India for his encouragement and permission to publish the research work.

CONTRIBUTORS

Mr Prabhat Sharma, received his BE from Govt. Engineering College Kota (Rajasthan Technical University, Kota), in 2000 and received his MTech from Indian Institute of Technology, Delhi, in 2011. Presently, he is working as a scientist in Instrument Research and Development Establishment, Dehradun and pursuing his PhD in the Department of Electronics and Communication Engineering at Indian Institute of Technology, Roorkee. His research interest include: RF signal processing, remote sensing and laser range sensor.
Contribution in the current study, he is main contributor of this study. He conceived the idea of current study and developed this algorithm.

Mr Bambam Kumar received his MTech in Integrated Electronics and Circuits from Indian Institute of Technology, Delhi in 2011 and pursuing the PhD in hidden object detection through Microwave and MMW imaging at the Indian Institute of Technology Roorkee (IIT Roorkee), Roorkee, India. He possesses more than 6 years of experience in teaching. He has received the Young Scientist award 2016 organised by UCOST, Uttarakhand. His research interests include : RF and microwave engineering, microwave and MMW imaging, and electromagnetic.
Contribution in the current study, he collected the data for various targets and simulated results during the development of this algorithm.

Dr Dharmendra Singh, received the PhD in Electronics Engineering from Banaras Hindu University, Varanasi, India. Currently working as a Professor with the Department of Electronics and Communication Engineering, IIT Roorkee, Roorkee, and a Coordinator of the RAILTEL IIT Roorkee Center of Excellence in Telecom, Roorkee. He has authored or co-authored over300 papers in various national/international journals and conferences. His main research interests include: Microwave remote sensing, electromagnetic wave interaction with various media, polarimetric and interferometric applications of microwave data, numerical modelling, ground penetrating radar, and through-wall imaging.
Contribution in the current study, he supervised all the activities of the current research work.